

# Structure and spin polarization of outermost surface of the $\text{Co}_2\text{FeAl}_{0.5}\text{Si}_{0.5}$ full-Heusler alloy studied by spin-polarized ion-scattering spectroscopy

T. T. Suzuki,\* H. Sukegawa, and K. Inomata

*National Institute for Materials Science, 1-2-1 Sengen, Tsukuba, Ibaraki 305-0047, Japan*

(Received 23 October 2008; published 27 January 2009)

The outermost surfaces of epitaxial full-Heusler  $\text{Co}_2\text{FeAl}_{0.5}\text{Si}_{0.5}$  (CFAS) films on MgO (001) substrates were investigated using spin-polarized ion-scattering spectroscopy. It was found that the CFAS surface was terminated by an Fe-Al-Si layer with substitution of Fe with Al and/or Si. The spin polarization of the outermost surface was detected for the first time among Heusler alloys. It was found that the spin polarization of Al and/or Si atoms in the topmost layer was significantly lower than that of Co atoms in the second layer. It was also found that the polarity of the spin polarization at the Fermi level on the outermost surface was opposite to majority spins. A possible application of SP-ISS in the development of magnetoresistance materials is suggested.

DOI: [10.1103/PhysRevB.79.045423](https://doi.org/10.1103/PhysRevB.79.045423)

PACS number(s): 68.49.-h, 34.80.Nz, 75.50.Cc

## I. INTRODUCTION

Recently, there has been a great deal of activity in the development of devices for spintronics such as magnetic tunnel junctions (MTJs). Half-metals that have 100% spin polarization at the Fermi level have been proposed as ideal candidates for spintronics devices. One class of such half-metals is Co-based full-Heusler alloys, which have the chemical formula  $\text{Co}_2YZ$  with an  $L2_1$  structure ( $Y$  and  $Z$  denote a transition metal and a main group element, respectively). This material is ideal because it seems to meet the requirements for practical use in magnetoresistive devices, such as high Curie temperature, large saturation magnetization, stability of the  $L2_1$  ordered structure, and large spin polarization at the Fermi level ( $P_{\text{EF}}$ ).

The spin polarization at the Fermi level,  $P_{\text{EF}}$ , is often used to characterize tunnel magnetoresistance (TMR). This is because the TMR ratio is directly related to  $P_{\text{EF}}$ , i.e.,  $2P_{\text{EF1}}P_{\text{EF2}}/(1-P_{\text{EF1}}P_{\text{EF2}})$ , where  $P_{\text{EF1}}$  and  $P_{\text{EF2}}$  denote  $P_{\text{EF}}$  of two ferromagnetic electrodes on either side of a nonmagnetic insulating layer in MTJs. As expressed in this relationship, first assumed by Julliere,<sup>1</sup> a larger TMR ratio is expected with larger  $P_{\text{EF}}$ . Since a larger TMR ratio is advantageous in possible applications using TMR, materials with larger  $P_{\text{EF}}$  have been desired. In this context, direct measurement of  $P_{\text{EF}}$  is essential in the development of magnetoresistance materials. Furthermore, it has been noted that the TMR ratio principally depends on  $P_{\text{EF}}$  at ferromagnetic/nonmagnetic interfaces.<sup>2</sup> Therefore, reliable measurements of  $P_{\text{EF}}$  at the surfaces and interfaces are important in the development of magnetoresistance materials. However, it is still difficult to measure  $P_{\text{EF}}$  even for bulk materials,<sup>3</sup> even more so for surfaces and interfaces. To the best of our knowledge, direct measurement of  $P_{\text{EF}}$  at surfaces and/or interfaces of Heusler alloys has not been reported so far.

Typically,  $P_{\text{EF}}$  has been estimated from magnetoresistance measurements using the Julliere model.<sup>1</sup> There are many parameters, such as film thickness, annealing temperature and fabrication conditions of a barrier, involved in the preparation of an MTJ. In addition, it usually takes times to complete the magnetoresistance measurement, which is per-

formed in ambient atmosphere, after preparation of the MTJ in vacuum. Thus, optimization of the growth conditions of magnetoresistance films has been a difficult task.

In the present study, we analyzed the structure and  $P_{\text{EF}}$  of the outermost surface of a  $\text{Co}_2\text{FeAl}_{0.5}\text{Si}_{0.5}$  (CFAS) full-Heusler alloy using an analytical method, spin-polarized ion-scattering spectroscopy (SP-ISS). In SP-ISS, electron spin-polarized  $^4\text{He}^+$  ions are projected on a sample surface, and the kinetic energy of scattered ions is analyzed.<sup>4</sup> The typical incident energy of  $\text{He}^+$  ions is on the order of keV, and therefore, most incident  $\text{He}^+$  ions are neutralized at the sample surface.<sup>5</sup> Since only scattered ions that survive this neutralization are detected, SP-ISS selectively observes only a few layers of the topmost surfaces. The spin dependence of ion neutralization, which typically occurs via the Auger neutralization (AN) process,<sup>6</sup> reflects the spin state of target atoms involved in collisions. The kinetic energy of the scattered ions depends on the mass of the target atoms,<sup>7</sup> and consequently, the element-selective spin state at the outermost surface is obtained by measuring the spin dependence of the neutralization probability as a function of scattering energy. Furthermore, atomic-layer-selective analysis is also expected by using shadow cones.<sup>8,9</sup>

In the AN process, surface electrons are emitted into the vacuum level. The intensity of the electron emission depends on the ion neutralization probability. Therefore,  $P_{\text{EF}}$  at the outermost surfaces can be estimated from the spin dependence of the electron emission [spin-polarized ion neutralization spectroscopy (SP-INS)].<sup>10,11</sup>

Figure 1 shows the crystal structure of CFAS with the  $L2_1$  ordered structure.<sup>12</sup> The space group is  $Fm\bar{3}m$ . The largest TMR ratio of up to 220% at room temperature has been reported for this composition among Co-based full-Heusler alloys.<sup>13</sup> As is clear from Fig. 1, if CFAS grows with the (100) plane, there are two possible termination layers at the outermost surface: the Co layer and the Fe-Al-Si layer. To our knowledge, there is no experimental report concerning structure analysis of this surface in Heusler alloy systems, including determination of the surface termination layer.

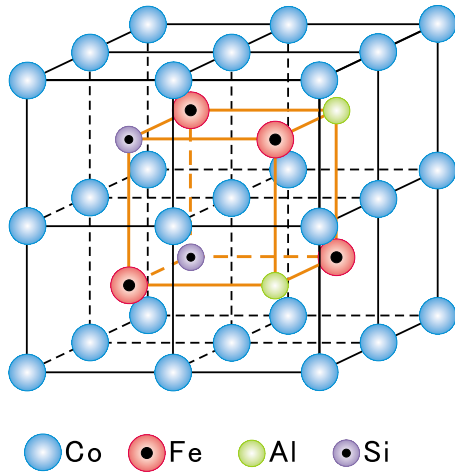


FIG. 1. (Color online) Ordered  $L2_1$  structure of  $\text{Co}_2\text{FeAl}_{0.5}\text{Si}_{0.5}$ .

## II. EXPERIMENTAL METHOD AND SETUP

### A. SP-ISS and SP-INS

In SP-ISS, spin-polarized  $\text{He}^+$  ions were projected on a sample surface, and the intensity of scattered  $\text{He}^+$  ions was measured using an electrostatic energy analyzer,<sup>4,14</sup> allowing the element-selective spin-state on the surface to be analyzed. On the other hand, the spin-resolved electronic state on the surface was analyzed by measuring electrons emitted from the decay process of spin-polarized  $\text{He}^+$  ions. This method is sometimes called SP-INS. In both SP-ISS and SP-INS, the spin direction of the incident  $\text{He}^+$  ions was either parallel or antiparallel to majority spins of the samples.

The details of our experimental setup have been described elsewhere.<sup>14,15</sup> Briefly, the spin-polarized  $\text{He}^+$  ions were generated from Penning ionization of spin-polarized  $\text{He } 2^3S_1$  atoms ( $\text{He}^*$ ), which were generated in an rf discharge.<sup>16</sup>  $\text{He}^*$  was spin polarized by optical pumping (OP).<sup>15</sup> In SP-ISS, the kinetic energy of the incident  $\text{He}^+$  ions and the scattering angle were set to 1.41 keV and  $150^\circ$ , respectively, in the present study. On the other hand, the kinetic energy of the projectiles was about 50 eV in SP-INS. The spin polarization of the  $\text{He}^+$  ions was determined from a comparison of the emitted electron spectra of  $\text{He}^+$  and  $\text{He}^{*10}$ . The CFAS sample was pulse-magnetized in-plane prior to measurements, where the magnetization direction was parallel to the CFAS [110] azimuth. In SP-ISS, both the incident and exit directions of the  $\text{He}^+$  ions were perpendicular to the magnetization, and therefore, the scattering plane contained both the surface normal and CFAS  $[1\bar{1}0]$  azimuth. The SP-ISS and SP-INS spectra were obtained using a rotatable hemispherical sector analyzer (Omicron SHA50). The measurements were performed with a constant pass of 40 eV for (SP-)INS and 318 eV for (SP-)ISS.

### B. CFAS film

We grew a CFAS film on a MgO (001) film homoepitaxially formed on a single crystalline MgO (001) substrate.<sup>17</sup> The base pressure of the chamber for film growth was below

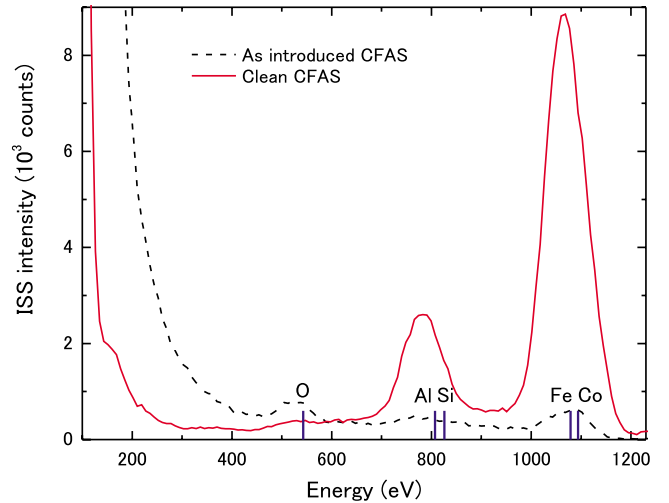


FIG. 2. (Color online) ISS spectra with normal incidence on the  $\text{Co}_2\text{FeAl}_{0.5}\text{Si}_{0.5}$  surface (a) before and (b) after surface cleaning.

$7 \times 10^{-10}$  Torr. The MgO (001) substrate was heated to 973 K for 1 h under vacuum. After cooling down to room temperature, a 20-nm-thick MgO layer was deposited on the substrate by rf sputtering directly from a sintered MgO target under an Ar pressure of 10 mTorr. After depositing the MgO layer, a 30-nm-thick CFAS thin film was subsequently deposited from a stoichiometric Co-Fe-Al-Si target (Co:50.0%, Fe:25.0%, Al:12.5%, and Si:12.5%). The Ar pressure during sputtering was 1.0 mTorr, and the typical deposition rate was  $2 \times 10^{-2}$  nm/s for CFAS. Finally, postdeposition annealing at 873 K was carried out after the CFAS film deposition.

After preparing the CFAS films, the sample was exposed to air followed by immediate introduction into the analysis chamber equipped with SP-ISS and reflection high-energy electron diffraction (RHEED) via a sample load-lock system. The base pressure of the analysis chamber was  $5 \times 10^{-11}$  Torr.

## III. RESULTS

Figure 2 shows ISS spectra obtained at the CFAS surface (a) before and (b) after surface cleaning. The cleaning procedure was several cycles of 2 keV  $\text{Ar}^+$  sputtering and annealing at 823 K. The incident angle measured from the surface normal was  $0^\circ$  (normal incidence). The binary collision energies (BCE) of  $\text{He}^+$  (1.41 eV) with Co, Fe, Si, Al, and O are indicated by bars at the bottom of the spectra. Since Fe and Co have close atomic weights, it is impossible to separate Fe and Co by ISS using the present setup. For the same reason, the separation of Si and Al is also difficult.

The surface peaks of ISS reflect the composition of a few surface layers. The ISS spectrum obtained before the surface cleaning (a) indicates that oxygen or oxides are one of the major contaminants on the surface. The strong background of secondary ions at the low energy side in the spectrum (a) is typical for surfaces contaminated with light molecules. This is probably due to the large sputtering rate of the contaminants. After sample cleaning, there were no peaks other than Fe-Co and Al-Si, except for the strong background of

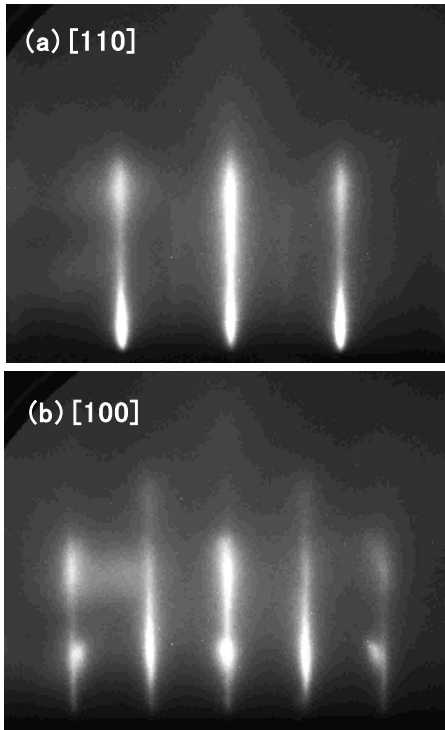


FIG. 3. RHEED patterns on the  $\text{Co}_2\text{FeAl}_{0.5}\text{Si}_{0.5}$  surface after surface cleaning along (a) [110] and (b) [100] azimuths.

secondary ions. It was observed that the intensity of the Fe-Co peak was much larger than that of the Al-Si peak. In ISS, element dependence of the peak intensity is attributed to the scattering cross section, surface composition, and neutralization probability of incident ions.<sup>7</sup> The substantially larger intensity of Fe-Co compared with Al-Si is reasonable, both from the scattering cross section and the surface composition. It was also observed that the background of secondary ions was drastically reduced by the sample cleaning. This is due to the relatively small sputtering rate of the surface constituents on the clean CFAS surface.

The surface peaks appear at slightly lower energy than BCE in Fig. 2. This is generally observed in ISS and is attributed to inelastic scattering accompanied with electronic-states excitation at the surface by the incident ions.

Figure 3 shows RHEED patterns on the CFAS surface along the (a) [110] and (b) [100] azimuths. The RHEED patterns show clear  $1 \times 1$  streaks, indicating the identical periodicity of the bulk crystal. The epitaxial orientation relationship was observed to be  $\text{CFAS}[110]//\text{MgO}[100]$  and  $\text{CFAS}(100)//\text{MgO}(100)$ . This is consistent with previous reports.<sup>13,17,18</sup> The ISS spectra in Fig. 2 and the RHEED patterns in Fig. 3 show the effectiveness of the sample cleaning procedure in the present experiment.

Figure 4 shows incidence angle scans of the scattered  $\text{He}^+$  ion intensity from Al-Si (702–886 eV) and Fe-Co (982–1182 eV). In these measurements, incidence angle relative to the surface normal was varied along the [100] and [110] azimuths. It was observed that the Al-Si intensity drastically increased at around  $75^\circ$ , and no intensity change was found with the variation in the incidence angle below  $75^\circ$ . This

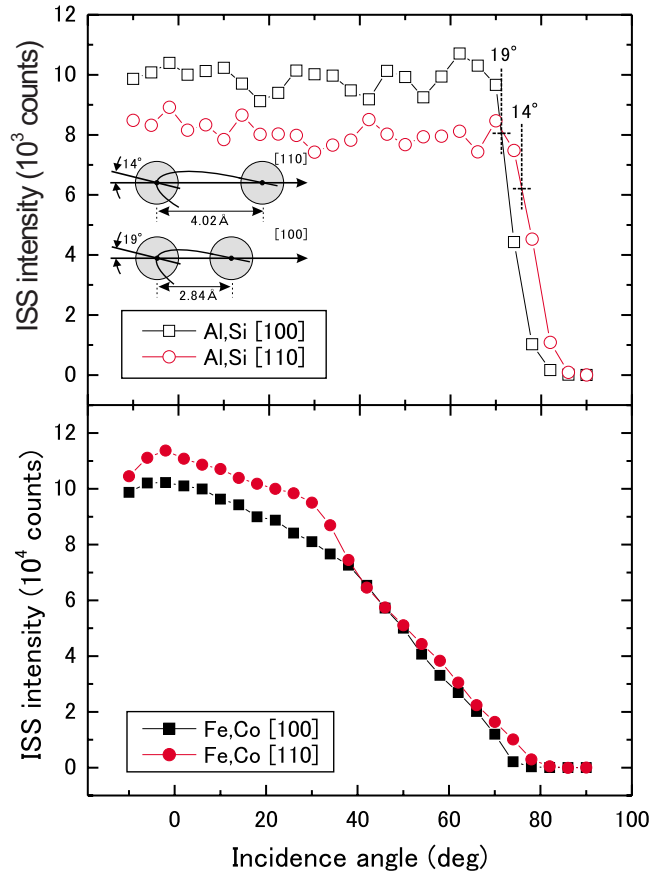


FIG. 4. (Color online) Incidence angle scan of ISS along [100] and [110] azimuths on the  $\text{Co}_2\text{FeAl}_{0.5}\text{Si}_{0.5}$  surface. The inset shows the atomic arrangement at the surface and the shadow cone.

intensity increase at around  $75^\circ$  is due to a focusing effect for Al and/or Si atoms located at the outermost surface.<sup>19</sup> The geometrical relationship between the atomic arrangement of the outermost surface and the shadow cone is schematically illustrated in the inset of Fig. 4, where the shadow cone was calculated using the Thomas-Fermi-Moliere potential.<sup>20</sup> It has been indicated that the critical angle of the focusing effect corresponds to the angle with 80%-maximum intensity.<sup>19</sup> The difference of the critical angle for the focusing effect between [100] ( $19^\circ$ ) and [110] ( $14^\circ$ ) is well explained from the distance between neighboring atoms in the bulk crystal structure, as shown in the inset.<sup>21</sup> This shows that the atomic position of the surface is identical to that of the bulk.

In contrast with Al-Si, no clear focusing peak was observed for Fe-Co in Fig. 2. Since the focusing effect at around  $75^\circ$  was likely due to atoms in the outermost surface layer, this straightforwardly indicates that both Fe and Co were not located in the outermost surface layer. Therefore, the surface termination layer was composed of only Al and Si. Accordingly, it is proposed that the CFAS surface is terminated by an Fe-Al-Si layer with substitution of Fe with Al and/or Si. If a vacancy occupies the Fe atom position at the outermost surface, the focusing effect should be observed at larger incidence angle compared with those observed for Al-Si in Fig. 4.<sup>5</sup> However, such a focusing effect is not observed in Fig. 4. Therefore, the possibility of substitution of

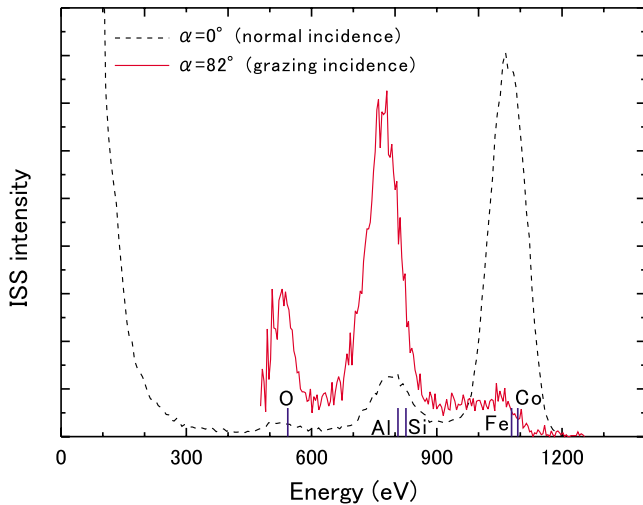


FIG. 5. (Color online) ISS spectra obtained on the  $\text{Co}_2\text{FeAl}_{0.5}\text{Si}_{0.5}$  with incidence angles of (a)  $0^\circ$  and (b)  $82^\circ$ .

Fe atoms with vacancies at the CFAS outermost surface is excluded.

Surface termination by the Al-Si layer is also clearly observed in the ISS spectra shown in Fig. 5. The contribution to the surface peak with normal incidence is mainly attributed to the outermost and second surface layers by considering a shadowing effect. The  $\text{He}^+$  ions that originated from deeper layers via multiple scattering may also have contributed to the surface peak. On the other hand, only the outermost surface contributed to the surface peak at the incidence angle of  $82^\circ$ . It was clearly observed that the Fe-Co peak intensity was much larger than that of Al-Si for the incidence angle of  $0^\circ$ . This relationship of the relative intensity is opposite for the incidence angle of  $82^\circ$ . Therefore, the ISS spectra in Fig. 5 support the determination of the surface termination layer derived from Fig. 4. From the structural analysis shown in Figs. 4 and 5, it was revealed that the CFAS surface terminated with Al-Si was energetically favored over that terminated with Co. Recently, Miura *et al.*<sup>22</sup> reported in their theoretical study that MnSi-terminated interfaces are thermodynamically stable as compared with Co-terminated interfaces in the  $\text{Co}_2\text{MnSi}/\text{MgO}(001)$  system. Further theoretical studies for CFAS surfaces are expected to discuss the origin of the surface termination by the Al-Si layer.

Figure 6 shows (a) an ISS spectrum, (b) an SP-ISS spectrum, and (c) SP-ISS spin asymmetry on the CFAS clean surface. The incidence angle was  $0^\circ$ . Thus, the major contribution to the surface peak was attributed to the outermost and second surface layers, as mentioned above. The ISS and SP-ISS intensities are defined here as  $I_\uparrow + I_\downarrow$  and  $I_\uparrow - I_\downarrow$ , respectively, where  $I_\uparrow$  and  $I_\downarrow$  denote the scattered  $\text{He}^+$  ion intensity polarized parallel and ant-parallel to the majority spins, respectively. On the other hand, the spin asymmetry is defined as  $(I_\uparrow - I_\downarrow) / [P_{\text{He}^+} \cdot (I_\uparrow + I_\downarrow)]$ , where  $P_{\text{He}^+}$  expresses the spin polarization of the incident  $\text{He}^+$  ion beam.

In the SP-ISS spectrum, clear spin dependence was observed at the Fe-Co and Al-Si peaks. The polarity of the SP-ISS peak was parallel to that of the majority spins. It was also observed that the spin asymmetry of Fe-Co was substan-

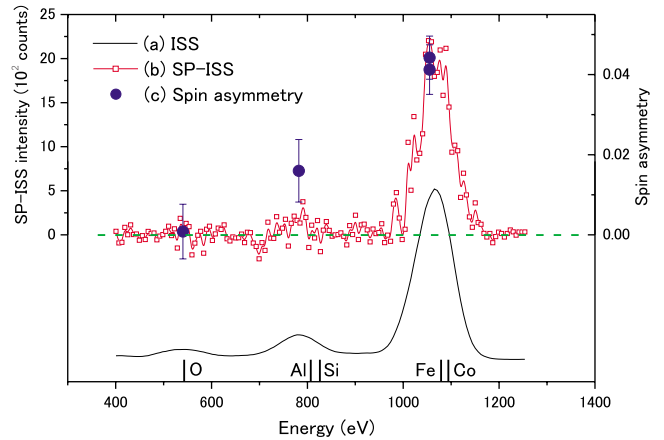


FIG. 6. (Color online) (a) ISS, (b) SP-ISS, and (c) SP-ISS spin asymmetry as a function of kinetic energy of scattered ions on the  $\text{Co}_2\text{FeAl}_{0.5}\text{Si}_{0.5}$  surface. The broken line shows zero-spin asymmetry.

tially larger than that of Al-Si, while almost no spin was induced in oxygen located at the topmost surface as a slight contaminant. The spin asymmetry reflects the spin polarization at the place where the incident  $\text{He}^+$  ions are neutralized.<sup>4</sup> Thus, the element-dependent spin asymmetry observed in Fig. 6 showed that the spin polarization of Co atoms in the second layer was substantially larger than that of Al and Si in the outermost surface layer. It was also indicated that almost no spin was induced in oxygen at the topmost surface. Furthermore, the spin direction of Co atoms was parallel to that of Al and Si judging from the polarity of the SP-ISS peaks.

Figure 7 shows an INS spectrum and an SP-INS asymmetry curve as a function of emitted electron energy. The incident and emitted angles measured from the surface normal were  $0^\circ$  and  $30^\circ$ , respectively. The origin of the emitted electrons with the largest kinetic energy was attributed to the Fermi level in AN, which is an interatomic two-electron process. Therefore, the SP-INS spin asymmetry at the Fermi level reflected  $P_{\text{FE}}$  at the outermost surface.

Secondary electrons from kinetic emission also contribute to the INS spectra, in addition to potential emission, such as

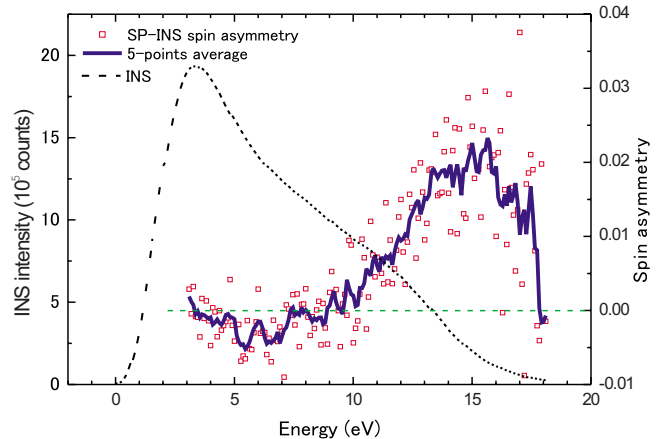


FIG. 7. (Color online) (a) INS, (b) SP-INS spin asymmetry, and (c) five-point average as a function of kinetic energy of emitted electrons on the  $\text{Co}_2\text{FeAl}_{0.5}\text{Si}_{0.5}$  surface.

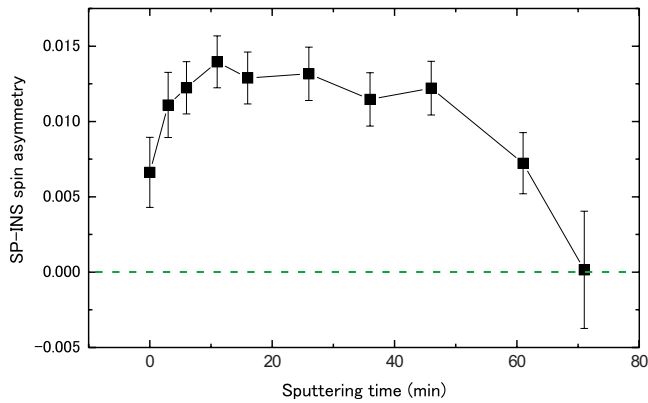


FIG. 8. (Color online) SP-INS spin asymmetry at  $E_F$  as a function of 2 keV  $\text{Ar}^+$  sputtering time on the  $\text{Co}_2\text{FeAl}_{0.5}\text{Si}_{0.5}$  surface. The broken line shows zero-spin asymmetry.

AN. It has been noted that the kinetic emission component acts as a background in SP-INS asymmetry curves.<sup>10</sup> To reduce this background, the incident  $\text{He}^+$  energy was reduced to about 50 eV for (SP-)INS measurements in the present study. However, judging from the substantial intensity above the Fermi level (about 15 eV), there should still be a non-negligible kinetic emission component. Actually, kinetic emission of electrons has been observed with  $\text{He}^+$  ions whose kinetic energy is below 30 eV.<sup>10</sup> Therefore, the SP-INS spin asymmetry at the Fermi level was substantially lower than  $P_{\text{EF}}$ .

The polarity of SP-INS spin asymmetry at the Fermi level is positive in Fig. 7, showing negative polarity of  $P_{\text{EF}}$  at the outermost surface. This is because the emitted electron intensity basically reflects the transition probability of surface electrons to the  $1s$  hole of the incident  $\text{He}^+$  ions, where the spin of the surface electrons should be antiparallel to that of the  $\text{He}^+$  ions. Thus, it is shown that the spin polarization at the Fermi level on the outermost surface was opposite to the majority spins of the CFAS. Several experimental studies have reported similar phenomena on Fe and Ni surfaces.<sup>23,24</sup> The spin at the Fermi level on the outermost surface in the opposite direction to the majority spin has theoretical support,<sup>25</sup> and it is generally attributed to low coordination of surfaces.

Figure 8 shows the SP-INS spin asymmetry at the Fermi level (about 15 eV) as a function of 2 keV  $\text{Ar}^+$  sputtering time. It was observed that the asymmetry increased with the sputtering time in the initial stage. This is attributed to removal of slight contaminants from the surface. This removal of contaminants is most likely completed within a few min-

utes, considering the current density of the sputtering ion beam, which was about  $10 \mu\text{A}/\text{cm}^2$ . Thus, further increase in the asymmetry up to about 10 min should be due to other factors, such as preferential sputtering and surface disordering. This is surprising since it has been generally accepted that the largest  $P_{\text{EF}}$  is expected with the higher crystallinity of the  $L2_1$  structure.<sup>26,27</sup> The asymmetry decreased with further sputtering and vanished at 70 min. This was due to the removal of the CFAS film itself, as inferred from the disappearance of the Fe-Co peak in the ISS spectrum (not shown).

The tracking of spin asymmetry as a function of surface treatment demonstrated in Fig. 8 suggests a possible application of SP-ISS in the development of magnetoresistance materials. Actually, the enlargement of  $P_{\text{EF}}$  on the CFAS surface by sputtering in Fig. 8 implies further increase in TMR ratio with optimization of the surface treatment. The measurement time for each asymmetry was several minutes. Thus, we consider that surface destruction by the incident ion beam is negligible in SP-ISS by taking an ion current density of several  $\text{nA}/\text{cm}^2$ .

One major drawback of SP-ISS (or SP-INS) may be that it is difficult to obtain absolute values of  $P_{\text{EF}}$  from the spin asymmetry. This is because the kinetic emission component, which reduces the spin asymmetry, is experimentally difficult to remove.<sup>10</sup> Therefore, SP-ISS (or SP-INS) may be appropriate for tracking the relative change in  $P_{\text{EF}}$ . Such measurements may be beneficial in optimizing the growth conditions of magnetoresistance materials.

#### IV. CONCLUSION

We investigated the outermost surfaces of  $\text{Co}_2\text{FeAl}_{0.5}\text{Si}_{0.5}$  using spin-polarized ion-scattering spectroscopy. From the structural analysis, it was found that the surface was terminated by an Fe-Al-Si layer in which Fe was substituted with Al and/or Si. Displacement of the surface atomic position, such as surface rumpling, was not observed. From magnetic structural analysis, it was found that spin polarization of Co atoms in the surface second layer was substantially larger than that of Al and/or Si in the outermost surface. The spin polarization at the Fermi level on the surface was detected by spin-polarized ion neutralization spectroscopy. The spin polarization tracking as a function of the surface treatment demonstrated in the present study suggests a possible application of this analytical technique in the development of magnetoresistance materials.

#### ACKNOWLEDGMENTS

This work was partially supported by PRESTO-JST and SENTAN-JST.

\*Corresponding author; suzuki.taku@nims.go.jp

<sup>1</sup>M. Julliere, Phys. Lett. **54A**, 225 (1975).

<sup>2</sup>M. Cinchetti, J.-P. Wustenberg, M. S. Albaneda, F. Steeb, A. Conca, M. Jourdan, and M. Aeschlimann, J. Phys. D **40**, 1544 (2007).

<sup>3</sup>R. J. Soulen, Jr., J. M. Byers, M. S. Osofsky, B. Nadgorny, T. Ambrose, S. F. Cheng, P. R. Broussard, C. T. Tanaka, J. Nowak, J. S. Moodera, A. Barry, and J. M. D. Coey, Science **282**, 85 (1998).

<sup>4</sup>T. Suzuki and Y. Yamauchi, Surf. Sci. **602**, 579 (2008).

- <sup>5</sup>M. Aono, Y. Hou, C. Oshima, and Y. Ishizawa, *Phys. Rev. Lett.* **49**, 567 (1982).
- <sup>6</sup>H. D. Hagstrum, *Phys. Rev.* **96**, 336 (1954).
- <sup>7</sup>H. H. Brongersma, M. Draxler, M. de Ridder, and P. Bauer, *Surf. Sci. Rep.* **62**, 63 (2007).
- <sup>8</sup>J. W. Rabalais, *Science* **250**, 521 (1990).
- <sup>9</sup>M. Katayama, E. Nomura, M. Kanekama, H. Soejima, and M. Aono, *Nucl. Instrum. Methods Phys. Res. B* **33**, 857 (1988).
- <sup>10</sup>T. Suzuki and Y. Yamauchi, *Phys. Rev. A* **77**, 022902 (2008).
- <sup>11</sup>T. Suzuki and Y. Yamauchi, *Nucl. Instrum. Methods Phys. Res. B* **256**, 451 (2007).
- <sup>12</sup>P. J. Webster, *J. Phys. Chem. Solids* **32**, 1221 (1971).
- <sup>13</sup>N. Tezuka, N. Ikeda, S. Sugimoto, and K. Inomata, *Jpn. J. Appl. Phys. Part 2* **46**, L454 (2007).
- <sup>14</sup>T. Suzuki and Y. Yamauchi, *Anal. Sci.* **24**, 81 (2008).
- <sup>15</sup>T. Suzuki and Y. Yamauchi, *Nucl. Instrum. Methods Phys. Res. A* **575**, 343 (2007).
- <sup>16</sup>D. L. Bixler, J. C. Lancaster, F. J. Kontur, R. A. Popple, F. B. Dunning, and G. K. Walters, *Rev. Sci. Instrum.* **70**, 240 (1999).
- <sup>17</sup>W. Wang, H. Sukegawa, R. Shan, T. Furubayashi, and K. Inomata, *Appl. Phys. Lett.* **92**, 221912 (2008).
- <sup>18</sup>N. Tezuka, N. Ikeda, A. Miyazaki, S. Sugimoto, M. Kikuchi, and K. Inomata, *Appl. Phys. Lett.* **89**, 112514 (2006).
- <sup>19</sup>M. Aono and R. Souda, *Jpn. J. Appl. Phys. Part 1* **24**, 1249 (1985).
- <sup>20</sup>O. S. Oen, *Surf. Sci.* **131**, L407 (1983).
- <sup>21</sup>T. M. Nakatani, A. Rajanikanth, Z. GerCSI, Y. K. Takahashi, K. Inomata, and K. Hono, *J. Appl. Phys.* **102**, 033916 (2007).
- <sup>22</sup>Y. Miura, H. Uchida, Y. Oba, K. Abe, and M. Shirai, *Phys. Rev. B* **78**, 064416 (2008).
- <sup>23</sup>Y. Yamauchi and M. Kurahashi, *Appl. Surf. Sci.* **169–170**, 236 (2001).
- <sup>24</sup>M. Onellion, M. W. Hart, F. B. Dunning, and G. K. Walters, *Phys. Rev. Lett.* **52**, 380 (1984).
- <sup>25</sup>R. Wu and A. J. Freeman, *J. Appl. Phys.* **73**, 6739 (1993).
- <sup>26</sup>S. Picozzi, A. Continenza, and A. J. Freeman, *Phys. Rev. B* **69**, 094423 (2004).
- <sup>27</sup>K. Inomata, M. Wojcik, E. Jedryka, N. Ikeda, and N. Tezuka, *Phys. Rev. B* **77**, 214425 (2008).